Author/s:
Sani, MA;Le Brun, AP;Rajput, S;Attard, T;Separovic, F

Title:
The membrane activity of the antimicrobial peptide caerin 1.1 is pH dependent

Date:
2023-03-21

Citation:
Sani, M. A., Le Brun, A. P., Rajput, S., Attard, T. & Separovic, F. (2023). The membrane activity of the antimicrobial peptide caerin 1.1 is pH dependent. Biophysical Journal, 122 (6), pp.1058-1067. https://doi.org/10.1016/j.bpj.2023.01.021.

The membrane activity of the antimicrobial peptide caerin 1.1 is pH dependent

Marc-Antoine Sani[a,*], Anton P. Le Brun[b], Sunnia Rajput[a], Troy Attard[a], and Frances Separovic[a,c,*]

[a] *Bio21 Institute, University of Melbourne, Melbourne, VIC 3010, Australia.*

[b] *Australian Centre for Neutron Scattering, Australian Nuclear Science and Technology Organisation, Kirrawee DC, NSW 2232, Australia.*

[c] *School of Chemistry, University of Melbourne, Melbourne, VIC 3010, Australia.*

* Corresponding author

Keywords: Histidine residues; Membrane-active peptides; Phospholipid bilayers; Solid-state NMR, Molecular dynamics simulation

Abstract

Antimicrobial peptides (AMPs) are an important class of membrane-active peptides that can provide alternatives or complements to classic antibiotics. Among the many classes of AMPs, the histidine-rich family is of particular interest since they may induce pH-sensitive interactions with cell membranes. The AMP caerin 1.1 (Cae-1), from Australian tree frogs, has three histidine residues and, thus we studied the pH-dependence of its interactions with model cell membranes. Using NMR spectroscopy and molecular dynamics (MD) simulations, we showed that Cae-1 induced greater perturbation of the lipid dynamics and water penetrations within the membrane interior in an acidic environment compared to physiological conditions. Using ^{31}P solid-state NMR, the packing, chemical environment, and dynamics of the lipid headgroup were monitored. ^{2}H solid-state NMR showed that Cae-1 ordered the acyl chains of the hydrophobic core of the bilayer. These results supported the MD data which showed that Cae-1 was mainly inserted within the lipid bilayer for both neutral and negatively charged membranes, with the charged residues pulling the water and phosphate groups inwards. This could be an early step in the mechanism of membrane disruption by histidine-rich AMPs and

indicated that Cae-1 acts via a transmembrane mechanism in bilayers of neutral and anionic phospholipid membranes, especially in acidic conditions.

Significance

Histidine-rich antimicrobial peptides (AMPs) are an important class of membrane-active peptides that may induce pH-sensitive interactions with cell membranes. The Australian tree frog AMP caerin 1.1 (Cae-1) has three histidine residues, which possibly modulate the interactions with eukaryotic and prokaryotic membrane systems. NMR and MD simulations showed that Cae-1 induced greater perturbation of the lipid dynamics and water penetrations within the membrane interior in an acidic environment compared to physiological conditions. Cae-1 was mainly inserted within the lipid bilayer structure of both neutral and negatively charged membranes, with the charged residues pulling the water inwards, which could be an early step in the mechanism of membrane disruption by histidine-rich AMPs.

Introduction

Antimicrobial peptides (AMPs) are a class of membrane-active peptides that interact strongly with the lipid membrane of prokaryotic cells (1,2). The main driving force for the membrane targeting activity of AMPs is the electrostatic interaction between negatively charged membrane lipids and positively charged amino acids. Indeed, and in particular for bacteria, prokaryotic cell membranes display a net negative charge due to a significant content of anionic phospholipids, such as phosphatidylglycerol (PG) (3,4), compared to eukaryotic cells which are mainly made of the zwitterionic phospholipid, phosphatidylcholine (PC). Cationic AMPs possess a net positive charge due to a high number of the basic residues, lysine and arginine, but also from the amino acid histidine that has an imidazole side chain with a pKa of *ca.* 6 (5). Thus, histidine-containing AMPs can carry additional positive charge per histidine residue at moderately acidic pH environments. Several histidine-containing AMPs have been shown to change their molecular interactions with lipid membranes depending on pH. Native AMPs, such as the piscidins (6,7), GAD (8), and *in silico* designed AMPs, such as C18G (9), AHH (10), have been studied at physiological or acidic pH and shown to modify their activity against bacteria and interactions with lipid membranes. In general, AMPs exhibited lower minimum inhibitory concentration (MIC) against bacteria at pH 5 than at physiological pH. *In vitro* assays showed that peptides with charged histidines tend to be less structured (mainly a

decrease in helicity) but disrupted lipid membrane integrity more based on dye leakage assays. The pH modulated charge state of AMPs can also have an impact on the charge state of the bacterial surface (11)

In this work, we investigated the impact of pH on the histidine-rich AMP, caerin 1.1 (Cae-1). Cae-1 is secreted on the skin of the Australian tree frog *Litoria* (12). It is an amphipathic peptide 25 amino acids in length containing 3 histidines (GLLSVLGSVAK**H**VLP**H**VVPVIAE**H**L-NH_2). Cae-1 adopts a kinked helical structure in the presence of lipid membranes with a hinge induced by two prolines (Pro^{15}, Pro^{19}) (13). Two histidines (His^{12}, His^{16}) are located on the hydrophilic side of the amphipathic helix (14) while the terminal histidine (His^{24}) is on the hydrophobic face (Fig. 1). The effect of the pH on the peptide interactions with neutral PC or negatively charged PC/PG lipid membranes was investigated by using solid-state NMR, neutron reflectometry and molecular dynamics simulations.

Materials and Methods

Materials

1,2-dimyristoyl-sn-glycero-3-phosphocholine (DMPC, M_W 678), perdeuterated-acyl chain 1,2-dimyristoyl-sn-glycero-3-phosphocholine (D_{54}-DMPC, M_W 732), 1,2-dimyristoyl-sn-glycero-3-phosphoglycerol (DMPG, MW 688) and perdeuterated-acyl chain 1,2-dimyristoyl-sn-glycero-3-phosphoglycerol (D_{54}-DMPG, M_W 742) were purchased from Avanti Polar Lipids (Alabaster, USA). Caerin 1.1 (GLLSVLGSVAKHVLPHVVPVIAEHL-NH_2; M_W 2584) was synthesized manually by solid phase peptide synthesis and purified by HPLC to a purity >95% (Fig. S1) using HCl instead of trifluoroacetic acid salt (16).

Solid-state NMR sample preparation

NMR samples to investigate the interactions of Cae-1 were prepared as followed:

For DMPC-only multilamellar vesicles, (MLVs) dimyristoyl-phosphatidylcholine (DMPC) was solubilized in chloroform/methanol (3:1 v/v) before removal of solvents under nitrogen flow and further dried under vacuum for 1 hr. The lipid film was then hydrated with either a buffer solution at pH 7 (HEPES 20 mM, NaCl 100 mM) or pH 5 (acetate 20 mM, NaCl 100

mM) containing the appropriate amount of Cae-1 to reach a lipid to peptide (L/P) molar ratio of 30:1, except for the peptide-free sample, and lyophilised overnight. The powders were then rehydrated with similar buffer without salt to reach a hydration level of 70%wt. Three freeze-thaw cycles were used to achieve sample homogeneity prior to packing into a 4 mm rotor (Bruker, Wissembourg, France).

For DMPC/DMPG MLV preparation, DMPC and acyl chain deuterated dimyristoyl-phosphatidylglycerol D_{54}-DMPG at a 4:1 molar ratio were co-solubilized in chloroform/methanol (3:1 v/v) and further processed as for DMPC MLVs.

Solid-state NMR experiments

NMR experiments were conducted on a 9.4 T wide-bore Bruker Avance-III HD NMR spectrometer (Wissembourg, France) equipped with a 4 mm triple-resonance MAS probe. The temperature of all experiments was maintained at 303 K.

Static ^{31}P NMR spectra were collected under 57 kHz SPINAL64 proton decoupling (17) using a Hahn spin-echo sequence (18), a $\pi/2$-pulse with a duration of 4.4 μs and an echo delay of 30 μs. A minimum of 2k transients were averaged at a spectral width of 125 kHz, and were Fourier transformed following zero-filling to 16k points and 75 Hz exponential line broadening. ^{31}P relaxation experiments were carried out under MAS at 9090 Hz. T_1 relaxation times were measured using the inversion recovery pulse sequence (19). Typical recycle delays were 6 s with variable τ-delay values between 0 and 6 s. T_2 relaxation times were measured with a rotor-synchronized Hahn spin-echo experiment with total echo delay (τ) values between 0.5 and 26 ms using integer multiples of the rotor period. Static ^{31}P NMR spectra were analyzed using Topspin 3.5 solids program. Relaxation times were calculated using non-linear curve fits of peaks integrals vs. τ.

Static ^{2}H experiments were performed using a composite pulse solid echo sequence (20). Operating conditions included 5.5 μs $\pi/2$-pulses, 40 μs echo delay and 0.5 s recycle time. A minimum of 32k transients were averaged at a spectral width of 500 kHz, and were Fourier transformed following zero-filling to 8k points and 100 Hz exponential line broadening. Static deuterium spectra were numerically de-Paked within NMRPipe (21) using the de-Paking macro. The de-Paked spectra were converted to order parameters by dividing the static splittings with the static coupling constant of 255 kHz (22).

Molecular dynamics (MD)

The starting conformation of Cae-1 was generated from NMR data (23). The CHARMM-GUI membrane builder (24,25) was then used to prepare the DMPC or DMPC/DMPG (4:1) bilayer systems with 200 molecules per leaflet within a rectangular box containing 100 mM of KCl salt and a 12.5 Å layer of water. Cae-1 peptides were distributed randomly in a transmembrane orientation with a L/P molar ratio of 30:1, corresponding to 200 DMPC lipids per leaflet and 13 Cae-1 peptides. Of the 13 Cae-1 peptides, two were oriented at 180° compared to the other 11 peptides (Fig. S4). The Charmm36 forcefield was used (26). Histidine residues were either singly or doubly protonated to model the ionization state expected at pH 5 or 7 and the peptide C-terminus was amidated to match the experimental conditions. This led to Cae-1 having a net charge of +1 at pH7 or +4 at pH 5. The minimization, equilibration and production runs were performed with the AMBER CUDA package (27) on a desktop machine fitting a GPU GeForce GTX 1080 titanium and a CPU with 12 cores.

Each system was first minimized for 1000 steps using the steepest descent method followed by 1000 steps of the conjugate gradient method with a 12 Å non-bonded interaction cut-off. The peptides and lipids were restrained with a 10 kcal.mol^{-1}.Å^2 and 2.5 kcal.mol^{-1}.Å^2 potential, respectively. Then, 1.6 ns equilibration MD simulations were run at 310 K, using decreasing positional restraints to maintain the peptide backbone and the lipid atom positions. All covalent bonds involving hydrogen atoms were constrained using the SHAKE algorithm (28) and the rigid internal geometry for TIP3P water molecules was constrained with the SETTLE algorithm (29). The system temperature was maintained at 303 K using a Langevin thermostat (30) with a 3 ps-1 collision frequency. The system pressure was controlled at 1 bar using a semi-isotropic Monte-Carlo barostat with a xy surface tension (0 dyne/cm). 50 production runs of 10 ns each were performed with each restart using the previous coordinates with random velocities. For all analysis, the first 100 ns of simulation were omitted, thus, the trajectories were analyzed using 400 frames at 1 ns interval. The lipid order profiles, water contacts, electron density profiles were thus calculated as an average of forty simulations each of 10 ns (40x 10 ns). The area per lipid and peptide tilt angle are presented as a continuous simulation, and averages calculated across the 40x10 ns simulations. For the area per lipid calculation, the peptide cross-section area was removed, using an averaged value of 125 Å for an helical peptide (31).

The MD trajectories were visualized and analyzed using VMD (32) with custom scripts and the CPPTRAJ (33) software and fitting procedures and plots were created in Gnuplot (http://sourceforge.net/projects/gnuplot).

Results

Interaction of Cae-1 with DMPC MLVs at pH 5 and pH 7

The impact of Cae-1 on the headgroup region of DMPC MLVs was more significant at pH 5. Cae-1 had no effect on the ^{31}P isotropic chemical shift of DMPC but slightly reduced the ^{31}P chemical shift anisotropy (CSA, using the Haeberlen tensor definition), especially at pH 5 (Fig. 2A, B and Table 1). At L/P of 30:1, no isotropic signal was observed in the static ^{31}P spectra, indicating that Cae-1 did not induce domains with rapid lipid re-orientation, such as toroidal pore or micellar structures, as often observed for AMPs (34,35). However, since the formation of such structures is concentration dependent, the chosen L/P may not be low enough to disrupt significantly the bilayer organisation (36). The dynamics of the lipid motions were monitored by measuring the ^{31}P relaxation rates under magic angle spinning (MAS) (Fig. 2C, D and Table 1) (35,37). Cae-1 did not significantly change the spin-lattice T_1 relaxation rate of DMPC at pH 7 but did increase it by *ca.* 15% at pH 5, which indicates a decrease in intensity of motions on the ns timescale, such as reduced lipid rotation along the lipid long axis. The presence of the peptide reduced the spin-spin T_2 relaxation rate by 32% at pH 5 and 18% at pH 7. T_2 is sensitive to motion on the μs-ms timescale, such as membrane wobbling or lipid diffusion, thus Cae-1 is slowing global lipid motions. Overall, ^{31}P NMR experiments showed that Cae-1 had a stronger impact on the headgroup of DMPC bilayers when the histidine residues are charged, with a decrease in fast and slow motions.

The impact of the peptide on the hydrophobic core of the bilayers was monitored using deuterated DMPC acyl chains via ^{2}H static NMR experiments. The de-Paked spectra were used to obtain the order parameter S_{CD} profile along the lipid acyl chain (Fig. 3) (38). Cae-1 uniformly increased the order of the DMPC acyl chains at both pH, which suggests that Cae-1 inserted across the DMPC bilayers regardless of the charge of the histidine residues. Furthermore, the ^{2}H spectra of D_{54}-DMPC acquired in the presence of Cae-1 displayed a single set of quadrupolar splittings, indicating that Cae-1 diffused sufficiently quickly to perturb homogeneously the bilayer hydrophobic core without forming more rigid/ordered domains. Ordering of the acyl chains was also observed via neutron reflectometry (NR) for DMPC

supported bilayers at pH 7 (Fig. S2-3). NR (Supp. Inf.) supported the insertion of the peptide into the hydrophobic core of the bilayer together with some water penetration into the interface also observed.

The molecular dynamics simulations were performed for 40x10 ns with Cae-1 peptides initially positioned in a transmembrane orientation at random positions and with a L/P molar ratio of 30:1, which translated to 200 DMPC lipids per leaflet and 13 Cae-1 peptides. Of the 13 Cae-1 peptides, two were oriented at 180° compared to the other 11 peptides in order to test if specific peptide-peptide interactions are more likely via parallel or antiparallel assembly (see Fig. S4). The location of the peptides was chosen by taking into consideration the NMR and NR experimental data suggesting deep penetration of Cae-1 into the lipid bilayers. The DMPC bilayer was simulated once, and the pH 7 and pH 5 simulations were run with neutral (*i.e.*, only N_{D1} is protonated, net charge +1) or charged (*i.e.*, both imidazole nitrogens are protonated, net charge +4) histidine residues, respectively. From the simulations, the peptide tilt angle lengthways of their long axis versus the bilayer normal, the electron density profile including those of the three histidine residues and their hydration shell, the lipid order profiles, and the areas per lipid were extracted as an average of the 40x10 ns simulations (Fig. 4 and Fig. S5). In the presence of Cae-1, water penetrated deeply into the headgroup of the bilayer with greater effect at pH 5. His^{12} and His^{24} remained at similar positions at pH 7 and at pH 5 but in the latter case the residues spanned a larger area. The area per lipid was slightly increased in the presence of Cae-1 at pH5 but similar at pH7 compared to the peptide-free DMPC bilayer. His^{16} exhibited a more central location at pH 7 but was distributed across two populations further away from the centre of the bilayer at pH 5. The number of water molecules surrounding the histidine residues (within 5 Å) was constant but significantly higher at pH 5, especially for His^{12} and His^{16} (Fig. S5). It is also worth noting that at pH 7, not all peptide histidine residues were near a phosphate group, but almost all were at pH 5 (Fig. S5). Furthermore, the charged Lys^{11} and Glu^{23} residues were slightly more hydrated at pH 5 with the cationic residue in proximity to ^{31}P atoms. Interestingly, the peptide tilt angles were not very dispersed, centred at *ca,* 35 deg., at pH 7 but displayed a large distribution at pH 5, centred at *ca.* 42 deg. (Fig. S6). Overall, the MD simulations showed similar effects on the DMPC bilayer dynamics and packing properties analogous to the NMR and NR (see Table S2) experimental data. MD simulations allowed investigation at greater atomic detail of the location of the peptides within the bilayer, which also showed stronger perturbation with the charged histidine residues. In particular, His^{12} and His^{16} seemed to displace water towards the centre, and likely shifted the transmembrane

orientation of Cae-1. However, since the MD simulations were not run for a very long time, it is unlikely that the systems had reached final equilibrium, and the observed perturbations may be transient, although they do support the experimental data.

Interaction of Cae-1 with DMPC/DMPG (4:1) MLVs at pH 5 and pH 7

Bacterial lipid membranes are mostly negatively charged due to high content of phosphatidylglycerol (PG) and, a much lesser amount, cardiolipin phospholipids (3). The impact of PG lipids on the interactions of Cae-1 at pH 5 and pH 7 was thus investigated similarly to the DMPC systems. The static ^{31}P NMR experiments did not exhibit any significant isotropic contribution, but the presence of Cae-1 slightly reduced the CSA regardless of the pH. The MAS ^{31}P spectra displayed small upfield shifts of *ca.* 0.05 ppm for DMPG but not so for DMPC (Fig. 5 and Table 1). Relaxation rates were perturbed similarly as for DMPC systems. T_1 values were longer in the presence of the peptide, especially for DMPG at pH 5 which exhibited the greatest change of *ca.* 29% compared to 10% for DMPC. T_2 values were shorter for DMPC but did not significantly change for DMPG. Thus, the overall effect of Cae-1 on the lipid headgroup of DMPC/DMPG bilayers was to reduce the slow and fast motions of the phosphate group, with more effect on the DMPG headgroup and when the histidine residues are charged. Thus electrostatic interactions appear to have higher impact on the charged membrane surface, as previously reported (39).

The perturbation of the DMPC/DMPG (4:1) MLVs hydrophobic core upon addition of Cae-1 was monitored using D_{54}-DMPG (Fig. 6). Deuteration of DMPG was chosen since stronger interactions between the negatively charged lipid and the positively charged peptide were anticipated, and ^{2}H signals would not be distinguishable if both lipids were deuterated. As for the D_{54}-DMPC systems, Cae-1 produced a significant increase in the order of the D_{54}-DMPG acyl chains. The ordering of the anionic lipid was sensed along the entire chain, thus indicating that Cae-1 remained inserted across the lipid bilayer also in the charged MLVs. Again, a single set of quadrupolar splittings was observed, signifying that all D_{54}-DMPG lipids were in a similar environment. At L/P 30:1 and a DMPC/DMPG molar ratio of 4:1, the DMPG/Cae-1 molar ratio is 6:1. Since the ^{31}P NMR data did not indicate much segregation of the PG lipids by Cae-1, as the chemical shift and relaxation rates of DMPC in the PC/PG bilayers did not tend towards those of the pure DMPC system, Cae-1 is also likely diffusing sufficiently quickly and homogenously perturbing the DMPC and D_{54}-DMPG lipids.

The MD simulations were performed as for the DMPC systems. The starting orientations of Cae-1 were identical, only the lipid systems changed with 160 DMPC and 40 DMPG used per leaflet. Overall, similar observations were obtained: the lipid headgroups tended to be more dispersed along the bilayer normal axis, moving inwards, and water penetrated deeper into the headgroup area (Fig. 7, Fig S7). The perturbation of the acyl chains of DMPC and DMPG by Cae-1 at both pH 5 and 7 were less pronounced than for the DMPC bilayer, and differed depending on the charge of the peptide. At pH 7, similar increases in the order parameter of DMPC and DMPG were observed but at pH 5, the order parameter of C1 to C6 near the glycerol region exhibited little perturbation for both DMPC and DMPG, while the rest of the chain carbons were ordered by the peptide, as was observed by ^{2}H NMR. The area per lipid increased in the presence of Cae-1 at pH 5 but not at pH 7 (Fig. 7), as observed with the DMPC bilayer. The hydration of the histidine residues and proximity of a phosphate group within 5 Å of the residue were also not much different to that found in the DMPC systems, regardless of the charge of Cae-1 (Fig. S7). Interestingly, the peptide tilt angles were more dispersed at pH 7 than was observed for the DMPC membrane system, while at pH 5 the same larger dispersion was measured (Fig. S8).

Discussion

AMPs are membrane active peptides, their primary target is the lipid membrane, and they have a greater preference for prokaryotic rather than eukaryotic membranes. However, it has been shown that their disruption of neutral membranes is greater despite a higher affinity for negatively charged membranes (40). Thus, electrostatic interactions are the driving force for AMP attraction towards cell membranes. Since several amino acids display an ionization state that is pH dependant, the impact of pH on AMP activity is of importance for the goal of using AMPs as antibiotic alternatives (41). Membrane permeabilizing peptides have been designed that become active at low pH and engineered to serve as intracellular carriers (42). Interestingly, histidine residues are commonly found in AMPs with similar frequency as for mammalian proteins (2.1% vs. 2.3%, respectively). Furthermore, over 35% of AMPs in the APD3 AMP database display at least one histidine residue with >15% having several (43) and Cae-1 having three histidines.

In the present study, Cae-1 did not drastically change its activity based on the charge of the lipid membrane, which was previously studied at pH 7 in DMPC and DMPC/DMPG (2:1) by

surface plasmon resonance and solid-state NMR (39). However, both membrane systems were more disturbed by Cae-1 at pH 5 than pH 7. The AMP primarily slowed the dynamics of the headgroup and hydrophobic core of the phospholipid membranes, likely as a result of inserting within the bilayers. Hence, it is unlikely that Cae-1 adopted a different orientation parallel or perpendicular to the bilayer normal, based on pH as reported for other membrane-active peptides, such as LAH4 (44) or GWALP23 (45). This is likely due to the high content of hydrophobic residues and the amphipathic structure of the helical Cae-1 (14,46). However, the MD simulations showed that, although maintaining an overall transmembrane orientation, the tilt angle fluctuation of the peptide long axis was significantly more distributed at pH 5 than pH 7. This was probably due to the greater exposure of the charged histidine residues to water, similarly to the snorkelling out effect seen with lysine and arginine residues (47-49). Furthermore, pH can also modify the ionization state and surface potential of the lipid membranes, which could also play a role in modulating the interactions with the cationic peptides (50,51). As often the case for amphipathic antimicrobial peptides, electrostatic and hydrophobic interactions are both playing a critical role in the peptide-lipid macromolecular assembly.

Note that in this study, the L/P ratio was fixed at 30:1. It is possible that the chosen ratio is not representative of the local peptide concentration that would be necessary to induce major disruption of the lipid bilayers. Increasing the peptide concentration is likely a prerequisite to trigger particular peptide-peptide assembly, such as transmembrane pores (52), as observed for pore-forming proteins (53). However, even below the minimum inhibition concentration for the AMP maculatin 1.1, transient pore formation in phospholipid bilayers and secondary targets in bacteria have been observed (54,55).

Conclusion

Although further investigations are necessary to fully characterize the pH dependence of Cae-1 in regard to its antimicrobial activity, the peptide does appear to act as transmembrane peptide in zwitterionic and anionic bilayers, and its effect is modulated by pH. Not only is the peptide concentration and charge state important parameters in peptide-peptide self-assembly, the lipid composition also plays a critical role for the interactions. As well as further studies in model membrane systems to characterize the mode of action, recent developments in in-cell NMR

allow studies of antimicrobial peptides in bacteria (54-58) or even proteins (59-62) within live cells.

AUTHOR CONTRIBUTIONS

M.-A. Sani and F. Separovic designed the research; M.-A. Sani, A. LeBrun, T. Attard, and S. Rajput performed the research and analyzed the data; M.-A. Sani, A. LeBrun, S. Rajput and F. Separovic wrote the manuscript; M.-A. Sani and F. Separovic edited the manuscript.

DECLARATION OF INTERESTS

The authors declare no competing interests.

Acknowledgments

This manuscript is dedicated to Dr Klaus Gawrisch, in honour of his contributions to membrane biophysics and NMR spectroscopy, and in appreciation for his many years of mentorship, encouragement and friendship.

This research was funded by the Australian Research Council (ARC) Discovery Project grant DP190101506 to F.S., DP210101792 to M.-A.S and LIEF grant LE160100120 to F.S and M.-A.S. NMR experiments were performed at the Bio21 Institute NMR facility and the peptide synthesis at the Bio21 Institute Melbourne Protein Characterization facility.

References

1. Sani, M. A., and F. Separovic. 2016. How Membrane-Active Peptides Get into Lipid Membranes. *Acc Chem Res*. 49(6):1130-1138, doi: 10.1021/acs.accounts.6b00074, https://www.ncbi.nlm.nih.gov/pubmed/27187572.
2. Jenssen, H., P. Hamill, and R. E. Hancock. 2006. Peptide antimicrobial agents. *Clin Microbiol Rev*. 19(3):491-511, doi: 10.1128/CMR.00056-05, https://www.ncbi.nlm.nih.gov/pubmed/16847082.
3. Kralj, T., M. Nuske, V. Hofferek, M. A. Sani, T. H. Lee, F. Separovic, M. I. Aguilar, and G. E. Reid. 2022. Multi-Omic Analysis to Characterize Metabolic Adaptation of the E. coli Lipidome in Response to Environmental Stress. *Metabolites*. 12(2), doi: 10.3390/metabo12020171, https://www.ncbi.nlm.nih.gov/pubmed/35208246.
4. Lee, T. H., V. Hofferek, M. A. Sani, F. Separovic, G. E. Reid, and M. I. Aguilar. 2021. The impact of antibacterial peptides on bacterial lipid membranes depends on

stage of growth. *Faraday Discuss*. 232(0):399-418, doi: 10.1039/d0fd00052c, https://www.ncbi.nlm.nih.gov/pubmed/34558564.
5. Hancock, R. E. 2001. Cationic peptides: effectors in innate immunity and novel antimicrobials. *Lancet Infect Dis*. 1(3):156-164, doi: 10.1016/S1473-3099(01)00092-5, https://www.ncbi.nlm.nih.gov/pubmed/11871492.
6. Mihailescu, M., M. Sorci, J. Seckute, V. I. Silin, J. Hammer, B. S. Perrin, Jr., J. I. Hernandez, N. Smajic, A. Shrestha, K. A. Bogardus, A. I. Greenwood, R. Fu, J. Blazyk, R. W. Pastor, L. K. Nicholson, G. Belfort, and M. L. Cotten. 2019. Structure and Function in Antimicrobial Piscidins: Histidine Position, Directionality of Membrane Insertion, and pH-Dependent Permeabilization. *J Am Chem Soc*. 141(25):9837-9853, doi: 10.1021/jacs.9b00440, https://www.ncbi.nlm.nih.gov/pubmed/31144503.
7. Chekmenev, E. Y., S. M. Jones, Y. N. Nikolayeva, B. S. Vollmar, T. J. Wagner, P. L. Gor'kov, W. W. Brey, M. N. Manion, K. C. Daugherty, and M. Cotten. 2006. High-field NMR studies of molecular recognition and structure-function relationships in antimicrobial piscidins at the water-lipid bilayer interface. *J Am Chem Soc*. 128(16):5308-5309, doi: 10.1021/ja058385e, https://www.ncbi.nlm.nih.gov/pubmed/16620079.
8. McDonald, M., M. Mannion, D. Pike, K. Lewis, A. Flynn, A. M. Brannan, M. J. Browne, D. Jackman, L. Madera, M. R. Power Coombs, D. W. Hoskin, M. L. Rise, and V. Booth. 2015. Structure-function relationships in histidine-rich antimicrobial peptides from Atlantic cod. *Biochim Biophys Acta*. 1848(7):1451-1461, doi: 10.1016/j.bbamem.2015.03.030, https://www.ncbi.nlm.nih.gov/pubmed/25839356.
9. Hitchner, M. A., L. E. Santiago-Ortiz, M. R. Necelis, D. J. Shirley, T. J. Palmer, K. E. Tarnawsky, T. D. Vaden, and G. A. Caputo. 2019. Activity and characterization of a pH-sensitive antimicrobial peptide. *Biochim Biophys Acta Biomembr*. 1861(10):182984, doi: 10.1016/j.bbamem.2019.05.006.
10. Kacprzyk, L., V. Rydengård, M. Mörgelin, M. Davoudi, M. Pasupuleti, M. Malmsten, and A. Schmidtchen. 2007. Antimicrobial activity of histidine-rich peptides is dependent on acidic conditions. *Biochimica et Biophysica Acta (BBA) - Biomembranes*. 1768(11):2667-2680, doi: https://doi.org/10.1016/j.bbamem.2007.06.020, https://www.sciencedirect.com/science/article/pii/S0005273607002362.
11. Walkenhorst, W. F., J. W. Klein, P. Vo, and W. C. Wimley. 2013. pH Dependence of microbe sterilization by cationic antimicrobial peptides. *Antimicrob Agents Chemother*. 57(7):3312-3320, doi: 10.1128/AAC.00063-13, https://www.ncbi.nlm.nih.gov/pubmed/23650166.
12. Wong, H., J. H. Bowie, and J. A. Carver. 1997. The solution structure and activity of caerin 1.1, an antimicrobial peptide from the Australian green tree frog, Litoria splendida. *Eur J Biochem*. 247(2):545-557, doi: 10.1111/j.1432-1033.1997.00545.x.
13. Pukala, T. L., M. P. Boland, J. D. Gehman, L. Kuhn-Nentwig, F. Separovic, and J. H. Bowie. 2007. Solution structure and interaction of cupiennin 1a, a spider venom peptide, with phospholipid bilayers. *Biochemistry*. 46(11):3576-3585, doi: 10.1021/bi062306+, https://www.ncbi.nlm.nih.gov/pubmed/17319697.
14. Sani, M. A., T. H. Lee, M. I. Aguilar, and F. Separovic. 2015. Proline-15 creates an amphipathic wedge in maculatin 1.1 peptides that drives lipid membrane disruption. *Biochim Biophys Acta*. 1848(10 Pt A):2277-2289, doi: 10.1016/j.bbamem.2015.06.013, https://www.ncbi.nlm.nih.gov/pubmed/26079051.

15. Kyte, J., and R. F. Doolittle. 1982. A simple method for displaying the hydropathic character of a protein. *J Mol Biol*. 157(1):105-132, doi: 10.1016/0022-2836(82)90515-0.
16. Sani, M. A., C. Loudet, G. Grobner, and E. J. Dufourc. 2007. Pro-apoptotic bax-alpha1 synthesis and evidence for beta-sheet to alpha-helix conformational change as triggered by negatively charged lipid membranes. *J Pept Sci*. 13(2):100-106, doi: 10.1002/psc.803, https://www.ncbi.nlm.nih.gov/pubmed/17106904.
17. Fung, B. M., A. K. Khitrin, and K. Ermolaev. 2000. An improved broadband decoupling sequence for liquid crystals and solids. *J Magn Reson*. 142(1):97-101, doi: 10.1006/jmre.1999.1896, https://www.ncbi.nlm.nih.gov/pubmed/10617439.
18. Kurnit, N. A., I. D. Abella, and S. R. Hartmann. 1964. Observation of a Photon Echo. *Physical Review Letters*. 13(19):567-568, doi: 10.1103/PhysRevLett.13.567, https://link.aps.org/doi/10.1103/PhysRevLett.13.567.
19. Drechsler, A., and F. Separovic. 2003. Solid-state NMR structure determination. *IUBMB Life*. 55(9):515-523, doi: 10.1080/15216540310001622740, https://www.ncbi.nlm.nih.gov/pubmed/14658757.
20. Spiess, H. W. 1974. Molecular motion studied by NMR powder spectra. I. Lineshape calculation for axially symmetric sheilding tensors. *Chemical Physics*. 6(2):217-225, doi: https://doi.org/10.1016/0301-0104(74)85062-7, https://www.sciencedirect.com/science/article/pii/0301010474850627.
21. Sani, M. A., D. K. Weber, F. Delaglio, F. Separovic, and J. D. Gehman. 2013. A practical implementation of de-Pake-ing via weighted Fourier transformation. *PeerJ*. 1:e30, doi: 10.7717/peerj.30, https://www.ncbi.nlm.nih.gov/pubmed/23638366.
22. Davis, J. H., M. Bloom, K. W. Butler, and I. C. Smith. 1980. The temperature dependence of molecular order and the influence of cholesterol in Acholeplasma laidlawii membranes. *Biochim Biophys Acta*. 597(3):477-491, doi: 10.1016/0005-2736(80)90221-7.
23. Wegener, K. L., J. A. Carver, and J. H. Bowie. 2003. The solution structures and activity of caerin 1.1 and caerin 1.4 in aqueous trifluoroethanol and dodecylphosphocholine micelles. *Biopolymers*. 69(1):42-59, doi: 10.1002/bip.10324, https://www.ncbi.nlm.nih.gov/pubmed/12717721.
24. Jo, S., T. Kim, V. G. Iyer, and W. Im. 2008. CHARMM-GUI: a web-based graphical user interface for CHARMM. *J Comput Chem*. 29(11):1859-1865, doi: 10.1002/jcc.20945, https://www.ncbi.nlm.nih.gov/pubmed/18351591.
25. Jo, S., T. Kim, and W. Im. 2007. Automated builder and database of protein/membrane complexes for molecular dynamics simulations. *PLoS One*. 2(9):e880, doi: 10.1371/journal.pone.0000880, https://www.ncbi.nlm.nih.gov/pubmed/17849009.
26. Lee, J., X. Cheng, J. M. Swails, M. S. Yeom, P. K. Eastman, J. A. Lemkul, S. Wei, J. Buckner, J. C. Jeong, Y. Qi, S. Jo, V. S. Pande, D. A. Case, C. L. Brooks, 3rd, A. D. MacKerell, Jr., J. B. Klauda, and W. Im. 2016. CHARMM-GUI Input Generator for NAMD, GROMACS, AMBER, OpenMM, and CHARMM/OpenMM Simulations Using the CHARMM36 Additive Force Field. *J Chem Theory Comput*. 12(1):405-413, doi: 10.1021/acs.jctc.5b00935, https://www.ncbi.nlm.nih.gov/pubmed/26631602.
27. Gotz, A. W., M. J. Williamson, D. Xu, D. Poole, S. Le Grand, and R. C. Walker. 2012. Routine Microsecond Molecular Dynamics Simulations with AMBER on GPUs. 1. Generalized Born. *J Chem Theory Comput*. 8(5):1542-1555, doi: 10.1021/ct200909j, https://www.ncbi.nlm.nih.gov/pubmed/22582031.
28. Gonnet, P., J. H. Walther, and P. Koumoutsakos. 2009. θ-SHAKE: An extension to SHAKE for the explicit treatment of angular constraints. *Computer Physics*

Communications. 180(3):360-364, doi: https://doi.org/10.1016/j.cpc.2008.10.020, https://www.sciencedirect.com/science/article/pii/S0010465508003676.
29. Miyamoto, S., and P. A. Kollman. 1992. Settle: An analytical version of the SHAKE and RATTLE algorithm for rigid water models. *Journal of Computational Chemistry*. 13(8):952-962, doi: https://doi.org/10.1002/jcc.540130805, https://onlinelibrary.wiley.com/doi/abs/10.1002/jcc.540130805.
30. Izaguirre, J. A., D. P. Catarello, J. M. Wozniak, and R. D. Skeel. 2001. Langevin stabilization of molecular dynamics. *The Journal of Chemical Physics*. 114(5):2090-2098, doi: 10.1063/1.1332996, https://aip.scitation.org/doi/abs/10.1063/1.1332996.
31. Hilderbrand, A. E., and D. E. Clemmer. 2005. Determination of sequence-specific intrinsic size parameters from cross sections for 162 tripeptides. *J Phys Chem B*. 109(23):11802-11809, doi: 10.1021/jp050761u, https://www.ncbi.nlm.nih.gov/pubmed/16852449.
32. Humphrey, W., A. Dalke, and K. Schulten. 1996. VMD: visual molecular dynamics. *J Mol Graph*. 14(1):33-38, 27-38, doi: 10.1016/0263-7855(96)00018-5.
33. Roe, D. R., and T. E. Cheatham, 3rd. 2013. PTRAJ and CPPTRAJ: Software for Processing and Analysis of Molecular Dynamics Trajectory Data. *J Chem Theory Comput*. 9(7):3084-3095, doi: 10.1021/ct400341p, https://www.ncbi.nlm.nih.gov/pubmed/26583988.
34. Bertelsen, K., J. Dorosz, S. K. Hansen, N. C. Nielsen, and T. Vosegaard. 2012. Mechanisms of peptide-induced pore formation in lipid bilayers investigated by oriented 31P solid-state NMR spectroscopy. *PLoS One*. 7(10):e47745, doi: 10.1371/journal.pone.0047745.
35. Sani, M. A., and F. Separovic. 2015. Progression of NMR studies of membrane-active peptides from lipid bilayers to live cells. *J Magn Reson*. 253:138-142, doi: 10.1016/j.jmr.2014.11.016, https://www.ncbi.nlm.nih.gov/pubmed/25631783.
36. Benfield, A. H., and S. T. Henriques. 2020. Mode-of-Action of Antimicrobial Peptides: Membrane Disruption vs. Intracellular Mechanisms. *Frontiers in Medical Technology*. 2, doi: 10.3389/fmedt.2020.610997, https://www.frontiersin.org/articles/10.3389/fmedt.2020.610997 (Mini Review).
37. Sani, M. A., and F. Separovic. 2018. Antimicrobial Peptide Structures: From Model Membranes to Live Cells. *Chemistry*. 24(2):286-291, doi: 10.1002/chem.201704362, https://www.ncbi.nlm.nih.gov/pubmed/29068097.
38. Molugu, T. R., X. Xu, A. Leftin, S. Lope-Piedrafita, G. V. Martinez, H. I. Petrache, and M. F. Brown. 2017. Solid-State Deuterium NMR Spectroscopy of Membranes. In Modern Magnetic Resonance. G. A. Webb, editor. Springer International Publishing, Cham, pp. 1-23.
39. Gehman, J. D., F. Luc, K. Hall, T. H. Lee, M. P. Boland, T. L. Pukala, J. H. Bowie, M. I. Aguilar, and F. Separovic. 2008. Effect of antimicrobial peptides from Australian tree frogs on anionic phospholipid membranes. *Biochemistry*. 47(33):8557-8565, doi: 10.1021/bi800320v, https://www.ncbi.nlm.nih.gov/pubmed/18652483.
40. Sani, M. A., E. Gagne, J. D. Gehman, T. C. Whitwell, and F. Separovic. 2014. Dye-release assay for investigation of antimicrobial peptide activity in a competitive lipid environment. *Eur Biophys J*. 43(8-9):445-450, doi: 10.1007/s00249-014-0970-0, https://www.ncbi.nlm.nih.gov/pubmed/24906225.
41. Malik, E., S. R. Dennison, F. Harris, and D. A. Phoenix. 2016. pH Dependent Antimicrobial Peptides and Proteins, Their Mechanisms of Action and Potential as Therapeutic Agents. *Pharmaceuticals (Basel)*. 9(4), doi: 10.3390/ph9040067.
42. Kim, S. Y., A. E. Pittman, E. Zapata-Mercado, G. M. King, W. C. Wimley, and K. Hristova. 2019. Mechanism of Action of Peptides That Cause the pH-Triggered

Macromolecular Poration of Lipid Bilayers. *J Am Chem Soc*. 141(16):6706-6718, doi: 10.1021/jacs.9b01970, https://www.ncbi.nlm.nih.gov/pubmed/30916949.
43. Wang, G., X. Li, and Z. Wang. 2016. APD3: the antimicrobial peptide database as a tool for research and education. *Nucleic Acids Res*. 44(D1):D1087-1093, doi: 10.1093/nar/gkv1278, https://www.ncbi.nlm.nih.gov/pubmed/26602694.
44. Wolf, J., C. Aisenbrey, N. Harmouche, J. Raya, P. Bertani, N. Voievoda, R. Suss, and B. Bechinger. 2017. pH-Dependent Membrane Interactions of the Histidine-Rich Cell-Penetrating Peptide LAH4-L1. *Biophys J*. 113(6):1290-1300, doi: 10.1016/j.bpj.2017.06.053, https://www.ncbi.nlm.nih.gov/pubmed/28734478.
45. Martfeld, A. N., D. V. Greathouse, and R. E. Koeppe, 2nd. 2016. Ionization Properties of Histidine Residues in the Lipid Bilayer Membrane Environment. *J Biol Chem*. 291(36):19146-19156, doi: 10.1074/jbc.M116.738583, https://www.ncbi.nlm.nih.gov/pubmed/27440045.
46. Fernandez, D. I., M. A. Sani, A. J. Miles, B. A. Wallace, and F. Separovic. 2013. Membrane defects enhance the interaction of antimicrobial peptides, aurein 1.2 versus caerin 1.1. *Biochim Biophys Acta*. 1828(8):1863-1872, doi: 10.1016/j.bbamem.2013.03.010, https://www.ncbi.nlm.nih.gov/pubmed/23506683.
47. Jafari, M., F. Mehrnejad, and F. Doustdar. 2017. Insight into the interactions, residue snorkeling, and membrane disordering potency of a single antimicrobial peptide into different lipid bilayers. *PLoS One*. 12(11):e0187216, doi: 10.1371/journal.pone.0187216, https://www.ncbi.nlm.nih.gov/pubmed/29125878.
48. Gibbons, W. J., Jr., E. S. Karp, N. A. Cellar, R. E. Minto, and G. A. Lorigan. 2006. Solid-state NMR studies of a diverged microsomal amino-proximate delta12 desaturase peptide reveal causes of stability in bilayer: tyrosine anchoring and arginine snorkeling. *Biophys J*. 90(4):1249-1259, doi: 10.1529/biophysj.105.067884, https://www.ncbi.nlm.nih.gov/pubmed/16326900.
49. Strandberg, E., S. Morein, D. T. Rijkers, R. M. Liskamp, P. C. van der Wel, and J. A. Killian. 2002. Lipid dependence of membrane anchoring properties and snorkeling behavior of aromatic and charged residues in transmembrane peptides. *Biochemistry*. 41(23):7190-7198, doi: 10.1021/bi012047i, https://www.ncbi.nlm.nih.gov/pubmed/12044149.
50. Lakhdar-Ghazal, F., J. L. Tichadou, and J. F. Tocanne. 1983. Effect of pH and monovalent cations on the ionization state of phosphatidylglycerol in monolayers. An experimental (surface potential) and theoretical (Gouy-Chapman) approach. *Eur J Biochem*. 134(3):531-537, doi: 10.1111/j.1432-1033.1983.tb07599.x, https://www.ncbi.nlm.nih.gov/pubmed/6884345.
51. Boggs, J. M., D. Stamp, and M. A. Moscarello. 1982. Effect of pH and fatty acid chain length on the interaction of myelin basic protein with phosphatidylglycerol. *Biochemistry*. 21(6):1208-1214, doi: 10.1021/bi00535a016, https://www.ncbi.nlm.nih.gov/pubmed/6176267.
52. Kim, S. Y., A.-N. Bondar, W. C. Wimley, and K. Hristova. 2021. pH-triggered pore-forming peptides with strong composition-dependent membrane selectivity. *Biophysical Journal*. 120(4):618-630, doi: https://doi.org/10.1016/j.bpj.2021.01.010, https://www.sciencedirect.com/science/article/pii/S0006349521000424.
53. Kisovec, M., S. Rezelj, P. Knap, M. M. Cajnko, S. Caserman, A. Flašker, N. Žnidaršič, M. Repič, J. Mavri, Y. Ruan, S. Scheuring, M. Podobnik, and G. Anderluh. 2017. Engineering a pH responsive pore forming protein. *Scientific Reports*. 7(1):42231, doi: 10.1038/srep42231, https://doi.org/10.1038/srep42231.

54. Sani, M. A., S. Zhu, V. Hofferek, and F. Separovic. 2019. Nitroxide spin-labeled peptides for DNP-NMR in-cell studies. *FASEB J*. 33(10):11021-11027, doi: 10.1096/fj.201900931R, https://www.ncbi.nlm.nih.gov/pubmed/31284743.
55. Separovic, F., V. Hofferek, A. P. Duff, M. J. McConville, and M. A. Sani. 2022. In-cell DNP NMR reveals multiple targeting effect of antimicrobial peptide. *J Struct Biol X*. 6:100074, doi: 10.1016/j.yjsbx.2022.100074, https://www.ncbi.nlm.nih.gov/pubmed/36147732.
56. Overall, S. A., S. Zhu, E. Hanssen, F. Separovic, and M. A. Sani. 2019. In Situ Monitoring of Bacteria under Antimicrobial Stress Using (31)P Solid-State NMR. *Int J Mol Sci*. 20(1), doi: 10.3390/ijms20010181, https://www.ncbi.nlm.nih.gov/pubmed/30621328.
57. Zhu, S., E. Kachooei, J. R. Harmer, L. J. Brown, F. Separovic, and M. A. Sani. 2021. TOAC spin-labeled peptides tailored for DNP-NMR studies in lipid membrane environments. *Biophys J*. 120(20):4501-4511, doi: 10.1016/j.bpj.2021.08.040, https://www.ncbi.nlm.nih.gov/pubmed/34480924.
58. Zhu, S., D. K. Weber, F. Separovic, and M. A. Sani. 2021. Expression and purification of the native C-amidated antimicrobial peptide maculatin 1.1. *J Pept Sci*. 27(8):e3330, doi: 10.1002/psc.3330, https://www.ncbi.nlm.nih.gov/pubmed/33843136.
59. Xiao, Y., R. Ghosh, and K. K. Frederick. 2021. In-Cell NMR of Intact Mammalian Cells Preserved with the Cryoprotectants DMSO and Glycerol Have Similar DNP Performance. *Front Mol Biosci*. 8:789478, doi: 10.3389/fmolb.2021.789478, https://www.ncbi.nlm.nih.gov/pubmed/35145995.
60. Ghosh, R., Y. Xiao, J. Kragelj, and K. K. Frederick. 2021. In-Cell Sensitivity-Enhanced NMR of Intact Viable Mammalian Cells. *J Am Chem Soc*. 143(44):18454-18466, doi: 10.1021/jacs.1c06680, https://www.ncbi.nlm.nih.gov/pubmed/34724614.
61. Overall, S. A., and A. B. Barnes. 2021. Biomolecular Perturbations in In-Cell Dynamic Nuclear Polarization Experiments. *Front Mol Biosci*. 8:743829, doi: 10.3389/fmolb.2021.743829, https://www.ncbi.nlm.nih.gov/pubmed/34751246.
62. Overall, S. A., L. E. Price, B. J. Albert, C. Gao, N. Alaniva, P. T. Judge, E. L. Sesti, P. A. Wender, G. B. Kyei, and A. B. Barnes. 2020. In Situ Detection of Endogenous HIV Activation by Dynamic Nuclear Polarization NMR and Flow Cytometry. *Int J Mol Sci*. 21(13), doi: 10.3390/ijms21134649, https://www.ncbi.nlm.nih.gov/pubmed/32629894.

Table 1 **^{31}P NMR parameters[a] of DMPC and DMPC/DMPG (4:1) MLVs upon interactions with Cae-1[b]**

	pH 5				pH 7			
	CS[c] (ppm)	CSA[c] (ppm)	T_1 (s)	T_2 (ms)	CS[c] (ppm)	CSA[c] (ppm)	T_1 (s)	T_2 (ms)
DMPC	-0.88	28.8	0.57 ± 0.01	11.71± 0.43	-0.90	26.9	0.84 ± 0.01	16.37± 0.58
+ Cae-1	-0.89	27.3	0.65 ± 0.01	8.01 ± 0.17	-0.89	26.8	0.83 ± 0.01	13.46 ± 0.50
DMPC/DMPG[d]	-0.80	25.7[e]	0.71 ± 0.01	7.60 ± 0.06	-0.85	25.1[e]	0.73 ± 0.01	7.21 ± 0.08
+ Cae-1	-0.78	24.1[e]	0.78 ± 0.01	6.25 ± 0.07	-0.84	24.1[e]	0.72 ± 0.01	5.96 ± 0.04
DMPC/DMPG[d]	0.26	25.7[e]	0.52 ± 0.01	5.84 ± 0.07	0.21	25.1[e]	0.56 ± 0.03	5.96 ± 0.17
+ Cae-1	0.32	24.1[e]	0.67 ± 0.01	5.82 ± 0.09	0.25	24.1[e]	0.60 ± 0.01	5.98 ± 0.06

[a] From experiments performed at 30°C. SD values obtained from curve fitting.

[b] Cae-1 added to MLVs at L/P 30:1

[c] CS: chemical shift; CSA: chemical shift anisotropy

[d] ^{31}P NMR values are for the underlined lipid.

[e] A single CSA was fitted for DMPC/DMPG and with Cae-1, as deconvolution of DMPC and DMPG was not possible. Value given according to the Haeberlen tensor definition.

Figure Captions

Figure 1 Helical wheel (left panel) display of Cae-1 with hydrophobic (yellow), polar (grey), basic (blue), acidic (red), proline (green) and histidine (light blue) residues. The hydrophobic moment is displayed with an arrow. NMR structure (right panel) of Cae-1 with color-coded hydrophobicity surface (blue - hydrophilic, white – neutral and red – hydrophobic) according to the Kyte and Doolittle scale (15).

Figure 2 A) Static, and B) MAS ^{31}P NMR spectra of D_{54}-DMPC MLVs (black lines) at pH 7 (top spectra) and pH 5 (bottom spectra) and in the presence of Cae-1 (red lines). C) T_1 spin-lattice relaxation, and D) T_2 spin-spin relaxation experiments with fitted lines (see Methods) obtained at 9 kHz. All experiments were performed at L/P 30:1 and at 30°C.

Figure 3 A) De-Paked ^{2}H NMR spectra of D_{54}-DMPC MLVs (black lines) at pH 7 (top spectra) and pH 5 (bottom spectra) and in the presence of Cae-1 (red lines), and (B, C) the corresponding lipid order profiles. All experiments were performed at L/P 30:1 and at 30°C.

Figure 4 Electron density profile obtained from 40x 10 ns simulations along the z axis (normal) of (A) the lipid bilayer, and in the presence of Cae-1: at (B) pH 7, and (C) pH 5. Phosphorous atoms (orange circles), water (cyan triangles), His^{12} (magenta crosses), His^{16} (pink squares) and His^{24} (purple inverted triangles) are depicted. (D) Order parameter profiles, and (E) area per lipid obtained from 40x 10 ns simulations of the DMPC bilayer (black triangles) and in the presence of Cae-1 at pH 7 (red squares) and pH 5 (blue circles). MD simulations were run at 303 K.

Figure 5 A) Static, and B) MAS ^{31}P NMR spectra of DMPC/D_{54}-DMPG (4:1) MLVs (black lines) at pH 7 (top spectra) and pH 5 (bottom spectra) and in the presence of Cae-1(red lines). T_1 spin-lattice relaxation experiments of C) DMPC, and D) D_{54}-DMPG. T_2 spin-spin relaxation experiments of E) DMPC, and F) D_{54}-DMPG with fitted lines (see Methods) obtained at 9 kHz MAS. All experiments were performed at L/P 30:1 and at 30°C.

Figure 6 A) De-Paked ^{2}H NMR spectra of DMPC/D_{54}-DMPG (4:1) MLVs (black lines) at pH 7 (top spectra) and pH 5 (bottom spectra) and in the presence of Cae-1 (red lines), and (B, C) corresponding lipid order profiles. All experiments were performed at L/P 30:1 and at 30°C.

Figure 7 Electron density profile obtained from 40x 10 ns simulations along the z axis (normal) of (A) the DMPC/DMPG (4:1) lipid bilayer, and in the presence of Cae-1 at (B) pH 7, and (C) pH 5. PC phosphorous atoms (orange circles), PG phosphorous atoms (red squares), water

(cyan triangles), His^{12} (magenta crosses), His^{16} (pink squares), and His^{24} (purple inverted triangles) are depicted. Lipid order parameter profiles for (D) DMPC, and (E) DMPG, and (F) area per lipid of the lipid bilayer (black triangles) and in the presence of Cae-1 at pH 7 (red squares) and pH 5 (blue circles) obtained from 40x 10 ns simulations. MD simulations were run at 303 K.

Figure 1

Click here to access/download;Figure;Fig 1.jpg

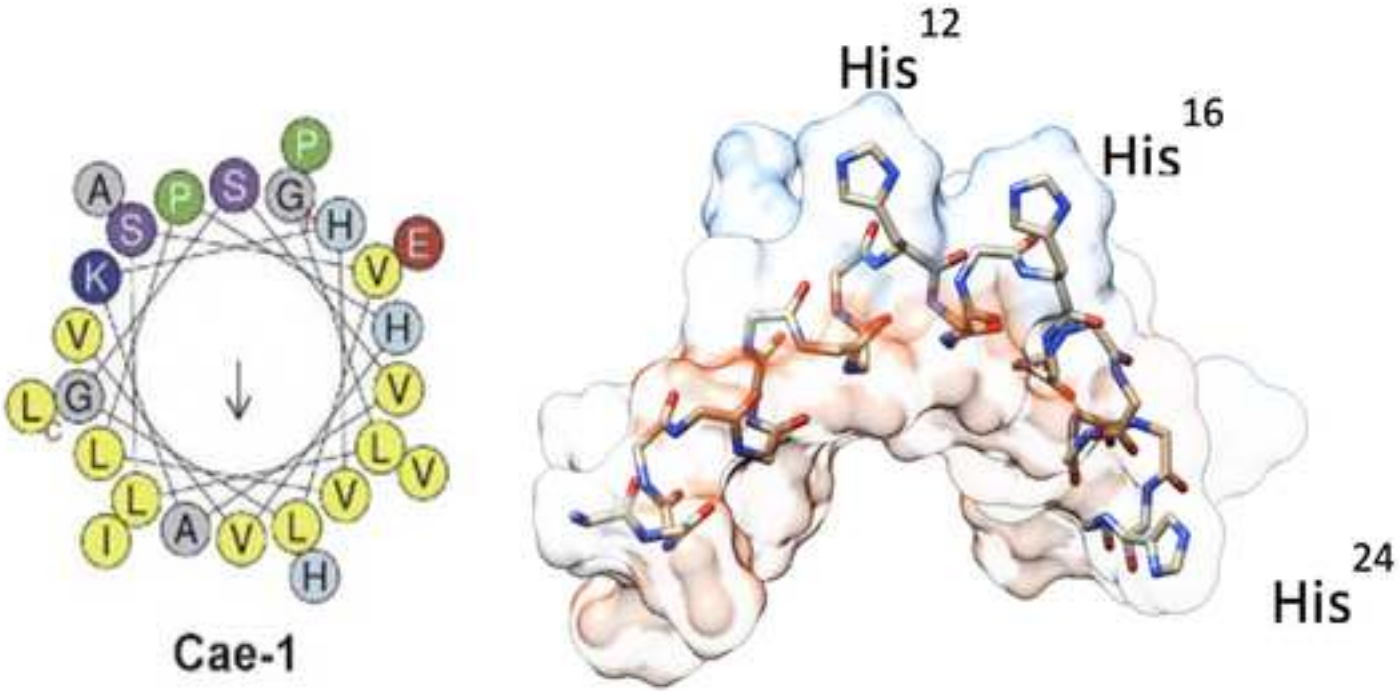

Figure 2

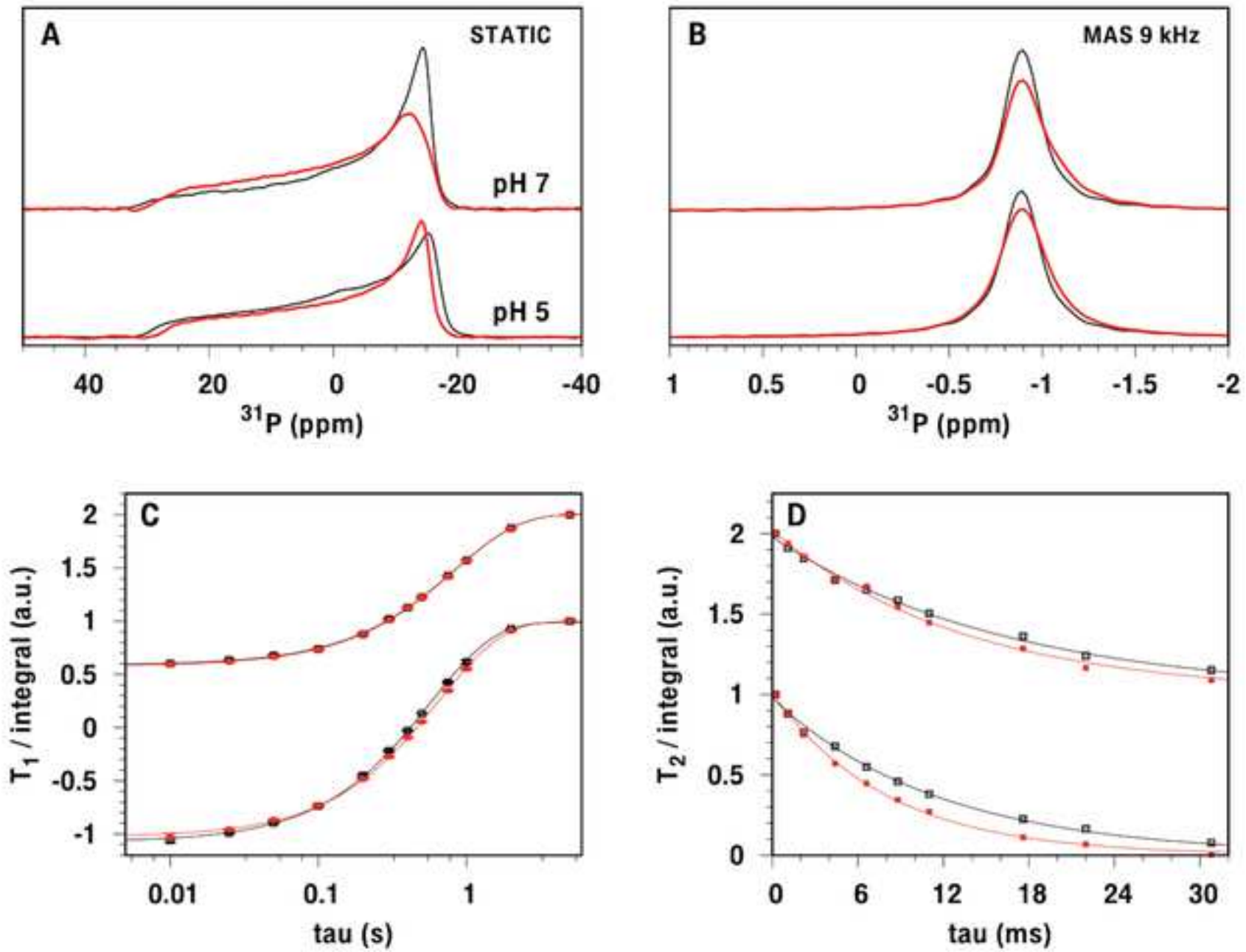

Figure 3

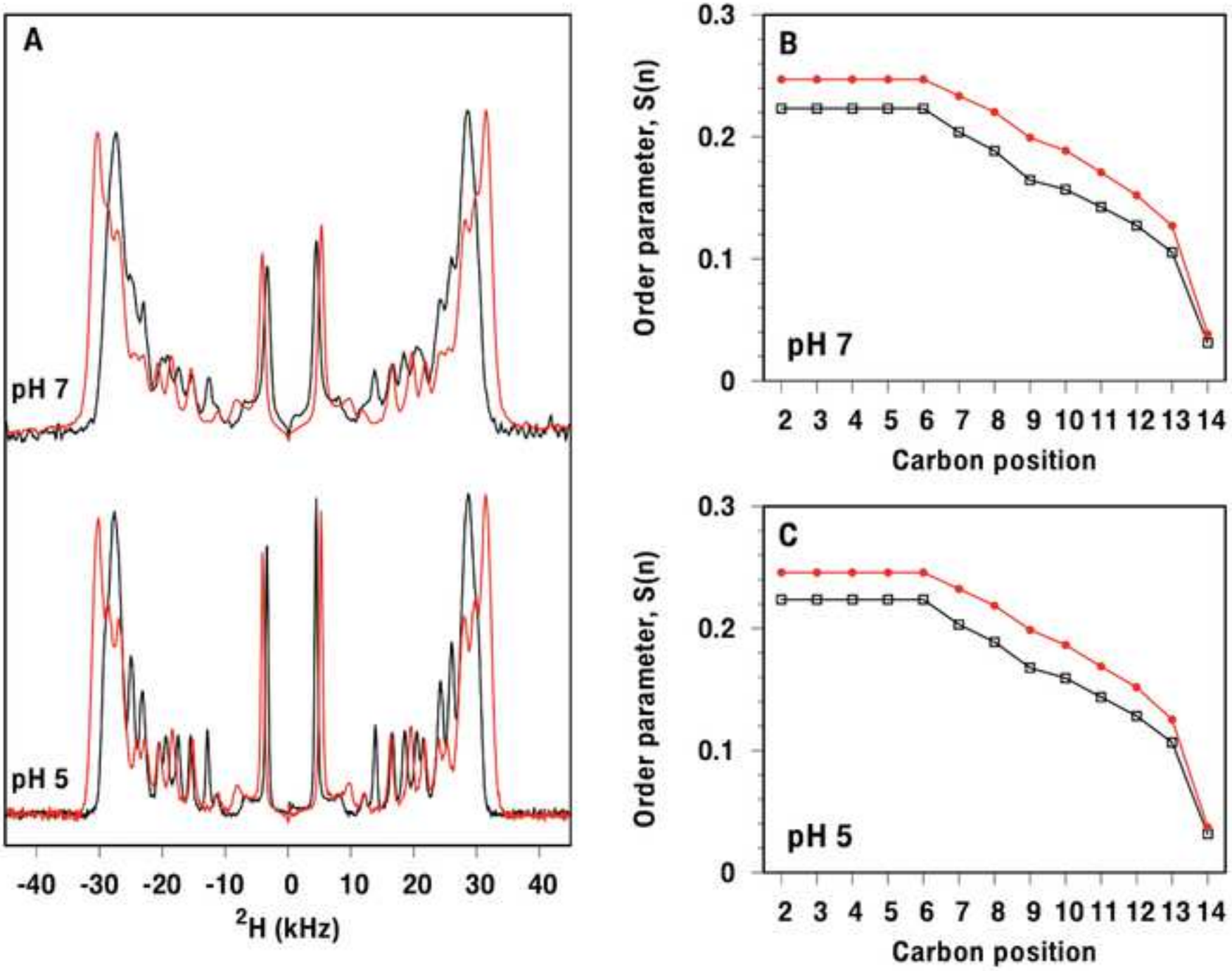

Figure 4

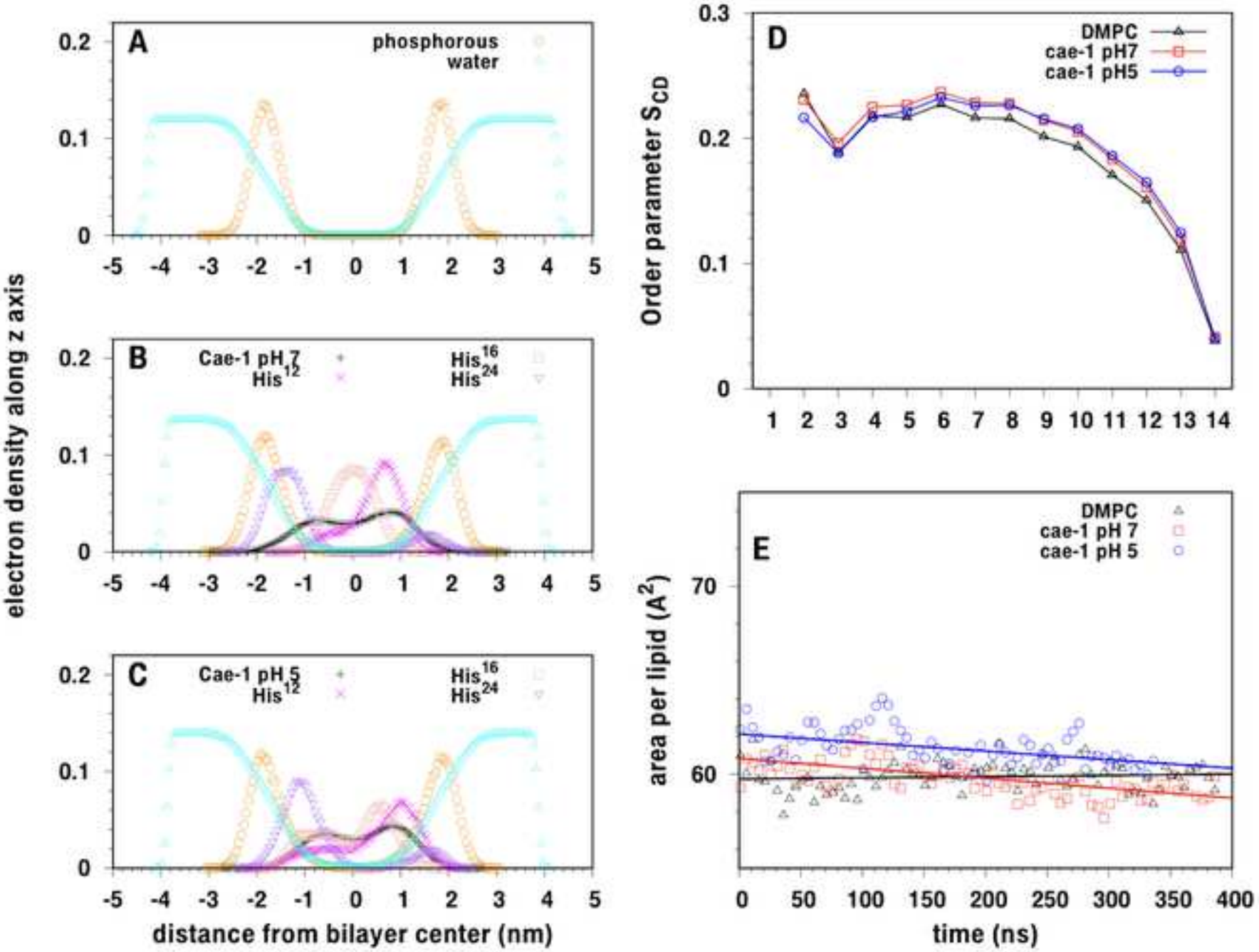

Figure 5

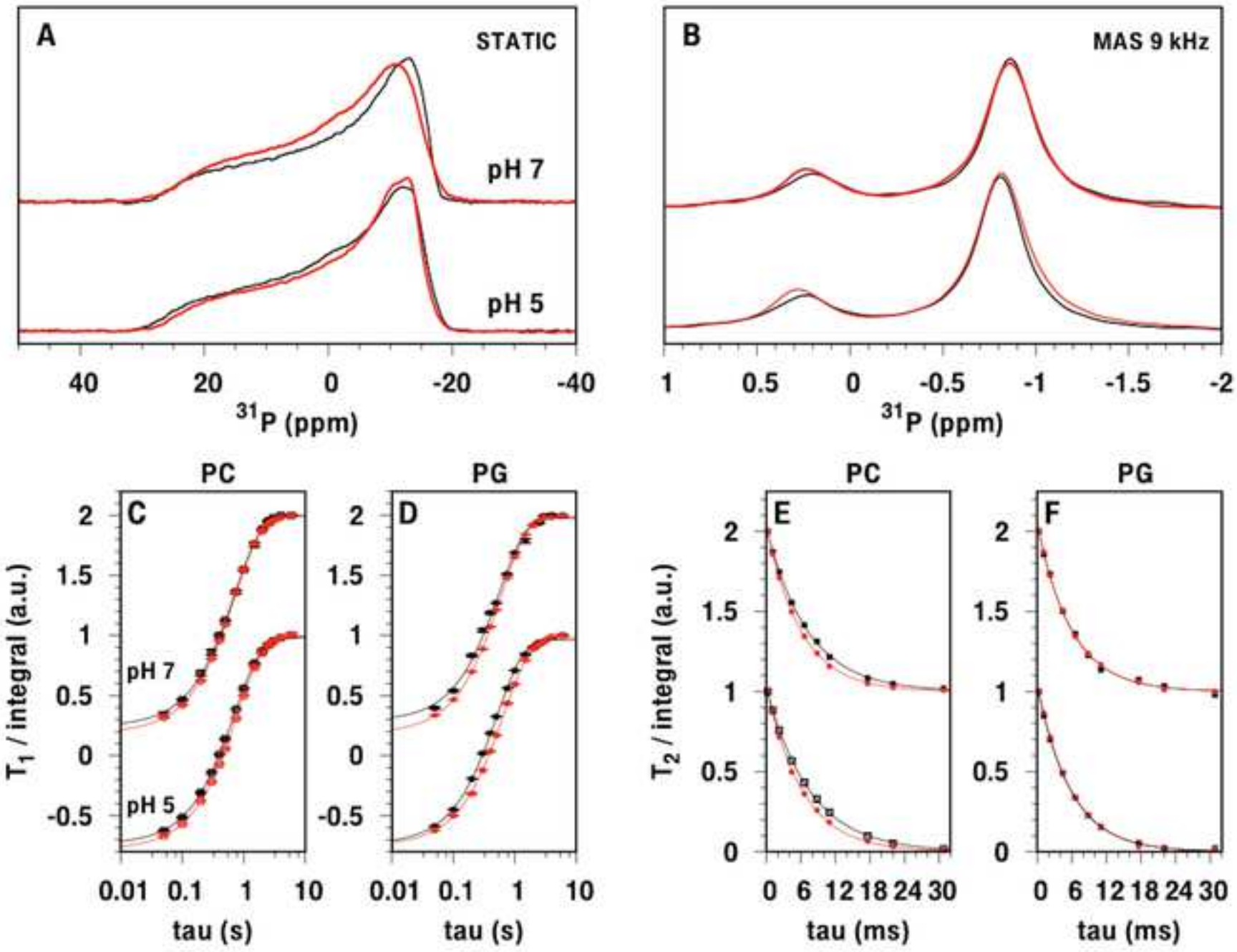

Figure 6

Click here to access/download;Figure;Fig 6.jpg

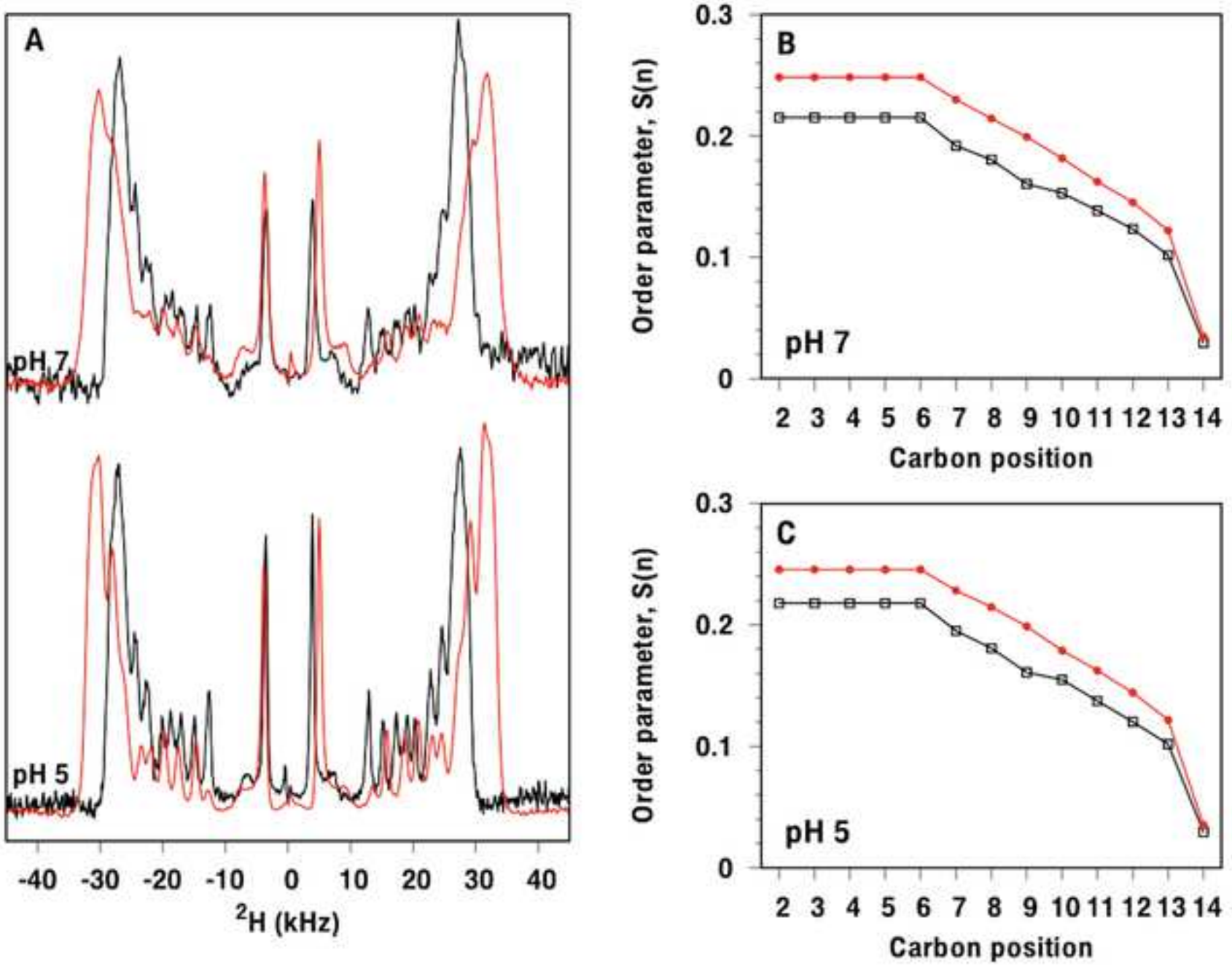

Figure 7